BIOCHEMISTRY
including biophysical chemistry & molecular biology

ARTICLE

pubs.acs.org/biochemistry

Quantum Mechanics/Molecular Mechanics Modeling of Substrate-Assisted Catalysis in Family 18 Chitinases: Conformational Changes and the Role of Asp142 in Catalysis in ChiB

Jitrayut Jitonnom,[*,†,‡] Vannajan S. Lee,[†] Piyarat Nimmanpipug,[†] Heather A. Rowlands,[‡] and Adrian J. Mulholland[*,‡]

[†]Computational Simulation and Modeling Laboratory (CSML), Department of Chemistry, Faculty of Science, Chiang Mai University, Chiang Mai, Thailand

[‡]Centre for Computational Chemistry, School of Chemistry, University of Bristol, Bristol BS8 1TS, U.K.

Supporting Information

ABSTRACT:

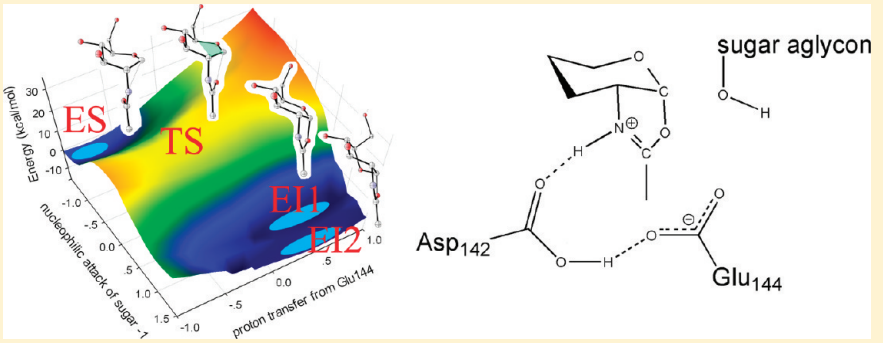

Family 18 chitinases catalyze the hydrolysis of β-1,4-glycosidic bonds in chitin. The mechanism has been proposed to involve the formation of an oxazolinium ion intermediate via an unusual substrate-assisted mechanism, in which the substrate itself acts as an intramolecular nucleophile (instead of an enzyme residue). Here, we have modeled the first step of the chitin hydrolysis catalyzed by *Serratia marcescens* chitinase B for the first time using a combined quantum mechanics/molecular mechanics approach. The calculated reaction barriers based on multiple snapshots are 15.8−19.8 kcal mol^{-1} [B3LYP/6-31+G(d)//AM1-CHARMM22], in good agreement with the activation free energy of 16.1 kcal mol^{-1} derived from experiment. The enzyme significantly stabilizes the oxazolinium intermediate. Two stable conformations ($^4C_1$-chair and $B_{3,O}$-boat) of the oxazolinium ion intermediate in subsite −1 were unexpectedly observed. The transition state structure has significant oxacarbenium ion-like character. The glycosyl residue in subsite −1 was found to follow a complex conformational pathway during the reaction ($^{1,4}B \rightarrow [^4H_5/^4E]^{\ddagger} \rightarrow {}^4C_1 \leftrightarrow B_{3,O}$), indicating complex conformational behavior in glycoside hydrolases that utilize a substrate-assisted catalytic mechanism. The D142N mutant is found to follow the same wild-type-like mechanism: the calculated barriers for reaction in this mutant (16.0−21.1 kcal mol^{-1}) are higher than in the wild type, in agreement with the experiment. Asp142 is found to be important in transition state and intermediate stabilization.

Glycoside hydrolases (GHs) (or glycosidases) are enzymes that hydrolyze glycosidic bonds (e.g., in carbohydrates) and are responsible for many important biological functions such as glycan processing in glycoproteins, remodeling the cell walls, and polysaccharide modification and degradation.[1] From work by Henrissat and co-workers[2] for sequence-based classification of these GHs, more than 110 GH families have been identified and are recorded in the carbohydrate-active enzymes (CAZy) server. These enzymes can be divided into two major classes, inverting and retaining GHs, whose reaction mechanisms differ in their stereochemical outcome (inversion or retention) with respect to configuration.[3−5] The reaction mechanisms of both inverting and retaining GHs involve acid−base chemistry and usually require two enzyme residues: one acting as a general acid and another acting as a general base or nucleophile, to catalyze the reaction efficiently. Specifically, the inverting enzymes act through a single-displacement mechanism that involves specifically positioned active site acid and base residues, whereas the retaining enzymes act through a double-displacement mechanism that in most cases involves acid−base and nucleophilic residues, which typically are carboxylic acid/carboxylate side chains of glutamic and/or aspartic acids; however, the retaining neuraminidases use a tyrosine residue as a catalytic nucleophile.[4]

Received: August 24, 2010
Revised: April 5, 2011
Published: April 07, 2011

Scheme 1. Proposed Substrate-Assisted Mechanisms for Retaining Glycoside Hydrolases (GHs) Involving a Potential Oxazoline/Oxazolinium Intermediate[6,17,19]

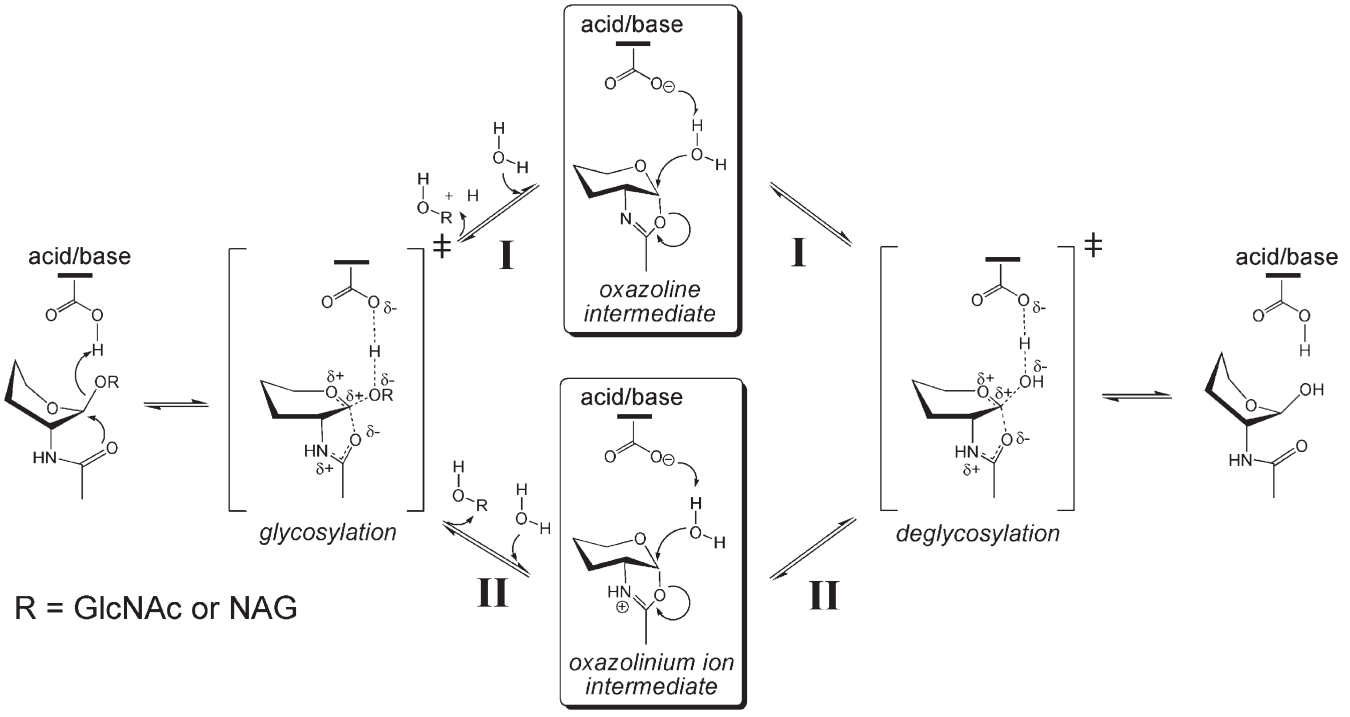

While the enzymic residue acts as nucleophile, some groups of retaining GHs do not need this amino acid residue; instead, they are widely thought to use the substrate itself as a nucleophile in the reaction, in an alternative mechanism for the glycosidic bond hydrolysis. This unusual mechanism is a "substrate-assisted" mechanism and is used by some retaining GHs that hydrolyze substrates containing an *N*-acetyl (acetamido) group at the C2 position, which is thought to act as an intramolecular nucleophile during catalysis.[6−8] Not all retaining GHs that cleave substrates bearing 2-acetamido groups do so via the substrate-assisted mechanism; for instance, hen egg white lysozyme[3,9] and enzymes of GH3[10] and GH22[11] utilize an enzymic nucleophile, rather than a 2-acetamido group. Other hexosaminidases such as GH19 enzymes[12] act through an inverting mechanism.

Members of families GH18 (chitinases), GH20 (chitobiases and hexosaminidases), GH56 (hyaluronidases), GH84 (O-GlcNAcases), and GH85 (endo-β-*N*-glucosaminidases) and probably GH25 lysozymes are retaining enzymes and are believed to share a common mechanistic feature of the substrate-assisted mechanism through the participation of the acetamido group (see Scheme 1). A structurally detailed understanding of this type of unusual mechanism could provide useful information for (e.g., structure-based) drug design for these enzymes, as they are related to numerous diseases such as asthma (GH18), Tay-Sachs and Sandhoff diseases (GH20), male infertility disorder (GH56), and Alzheimer's disease (GH84),[13] making them potentially attractive targets for drug discovery.

The substrate-assisted mechanism of those retaining GH enzymes involving a potential oxazoline/oxazolinium intermediate has previously been proposed on the basis of kinetic measurements and crystallographic structures[6,14−19] and can be divided into two possible reaction pathways (I and II, Scheme 1) which may be pH-dependent variants. These reaction pathways differ in only the formation of the intermediate, i.e., oxazoline or oxazolinium. The reaction consists of two discrete steps (glycosylation and deglycosylation) that require two key carboxylate groups (usually an aspartate or glutamate residue) that have been shown to be important in catalysis.[17−19] During the first step (glycosylation), a protonated carboxylic acid residue (Asp or Glu) that donates a hydrogen bond to the glycosidic oxygen acts as a general acid, facilitating glycosidic bond cleavage by protonating the oxygen atom of the departing aglycon moiety.[6−8] Nucleophilic attack at the anomeric center by the carbonyl oxygen of the 2-acetamido group is thought to displace the aglycon leaving group,[20] in a manner similar to that of the enzymic nucleophile of the more typical retaining GHs. This is believed to result in the formation of an oxazoline/oxazolinium intermediate via a ring closing (cyclization) reaction. The acetamido group is oriented, and its nucleophilicity at the anomeric center is thought to be enhanced, through donation of a hydrogen bond to a second suitably positioned carboxylate residue.[14,19] The role of this residue, however, has been debated, in particular whether it acts as a general acid/base to aid in formation of the oxazoline intermediate (suggested for GH84)[17] or, alternatively, to stabilize the oxazolinium ion intermediate electrostatically (proposed for GH18, GH20, GH56, and GH85).[6,14,19,20] During the second step (deglycosylation), the resulting intermediate is broken down in a reverse of the first step; the general acid residue in the first step is proposed to act as a general base, promoting the attack of an incoming water. This water molecule facilitates the departure of the 2-acetamido group from the anomeric center, yielding the sugar hemiacetal product with overall retention of stereochemistry.

Important questions regarding this proposed mechanism include the following. What conformation is adopted at the transition state? Are conformational changes of the pyranose ring necessary, and does the itinerary follow Stoddart's diagram[21] (which gives an idea of the possible conformational routes that might be followed by a

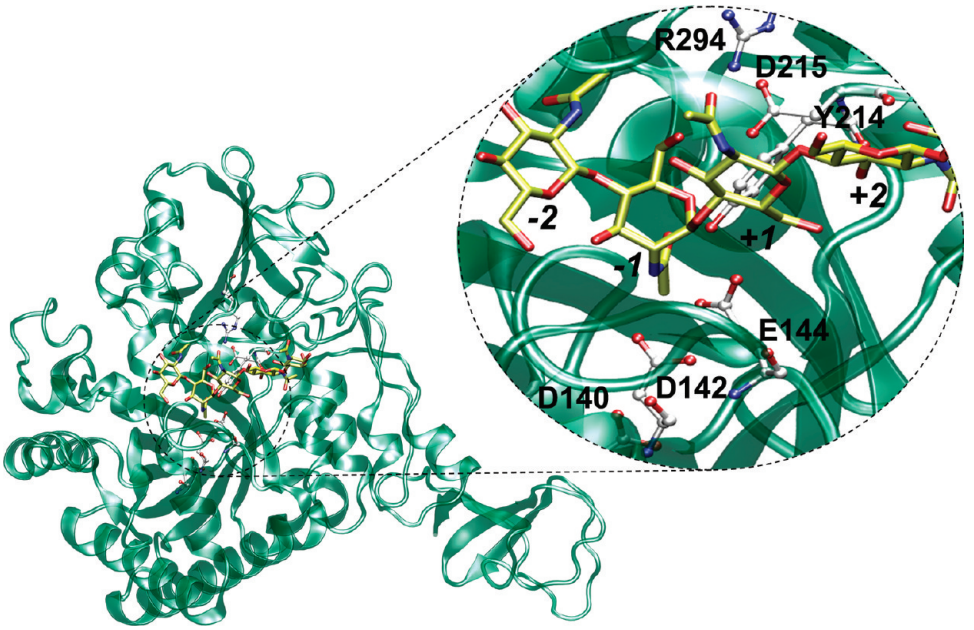

Figure 1. Enzyme−substrate complex of S. marcescens GH18 chitinase B (ChiB) (PDB entry 1E6N). The Gln144 residue of the crystal structure was mutated back to Glu here. The sugars bound to subsites −2 to +3 are drawn in a stick model with yellow carbon atoms, whereas the catalytic residues (Asp140, Asp142 and Glu144) and residues that contribute the hydrogen bonds to the sugar in subsite −1 and +1 are shown in a ball and stick model with white carbon atoms.

pyranoside ring as it moves from one conformation to another)? What are the structural and energetic details of the reaction pathway and catalytic mechanism? What are the roles of conserved residues in catalysis, especially for potentially stabilizing residues, e.g., Asp142 (GH18 chitinase B) or Asp174 (GH84 O-GlcNAcase)? How concerted is the reaction; e.g., does the acetamido group function by cooperating with a general acid residue to break the glycosidic bond, or is the glycosidic bond broken residue followed by nucleophilic attack of the acetamido group? Computational enzymology methods[22] can complement experiments in addressing these questions and revealing more details of this unusual mechanism.

Combined QM/MM (quantum mechanics/molecular mechanics) approaches, introduced for enzyme reactions by Warshel and Levitt,[23] treat the central reacting system with a quantum chemical method, while representing the remainder of the system by an empirical force field model.[24] Such methods can test proposed reaction mechanisms and elucidate details of structures and stabilization of transition states and intermediates at a level of detail that is beyond what can be achieved by experimental methods. QM/MM molecular simulations can identify and analyze interactions responsible for stabilizing such crucial species in enzymes. An example of the application of QM/MM methods to glycoside hydrolases is a study of hen egg white lysozyme that supports a covalent intermediate.[9] QM/MM methods[24] have been applied to study reaction mechanisms in several GH enzymes, e.g., lysozyme,[9] endoglucanase,[25] xylanase,[26,27] β-galactosidase,[28] cellulase,[29] and Golgi α-mannosidase.[30] However, to the best of our knowledge, none have previously investigated in detail the reaction mechanism of the GH families involving a potential oxazoline or oxazolinium ion intermediate formed by the substrate-assisted mechanism.

Modeling of enzyme-catalyzed reaction mechanisms ideally requires a good quality starting structure,[31] to represent the enzyme−substrate (ES) complex. Structures of complexes with mechanism-based inhibitors may in some cases be quite different from substrate complexes. van Aalten and co-workers[6] have reported a crystal structure of E144Q mutant chitinase B (ChiB) from *Serratia marcescens* in a complex with a penta-*N*-acetyl-chitopentaose substrate (Figure 1), providing a good starting structure of the enzyme-substrate complex for QM/MM modeling. Here, we study *S. marcescens* ChiB. This enzyme is important in its own right and as a representative case of substrate-assisted catalysis, potentially relating to other GH families (e.g., GH20, GH56, GH84, and GH85).

ChiB is a member of the GH18 family (chitinases). It degrades chitin, a linear insoluble polymer of β-(1,4)-linked *N*-acetylglucosamine (GlcNAc or NAG), which is the second most abundant biopolymer on earth after cellulose.[32] This enzyme has received much attention as an attractive model system for the development of new inhibitors[33] with possible chemotherapeutic potential against fungi, against the transmission of malaria, in insecticides, or as an anti-inflammatory for asthma and allergy diseases. Furthermore, this enzyme has been targeted in biotechnology for conversion of insoluble polysaccharides.[34] Mutation studies[18] indicate possible roles for many conserved residues (e.g., Tyr10, Ser93, Asp140, Asp142, Glu144, Tyr214, and Asp215). However, the mechanistic roles of these conserved residues are still unclear. Of particular interest is the role of Asp142: replacement of Asp142 with alanine in ChiB almost abolishes enzymatic activity, whereas the D142N mutant retains significant activity,[18] leading to the proposal that the reaction in the D142N mutant proceeds via a wild-type-like catalytic mechanism.[18,35]

In this study, we apply a combined QM/MM method to generate potential energy surfaces (PESs), find transition state (TS) and intermediate (EI) structures, and to identify and analyze interactions responsible for stabilizing the crucial species (ES, TS, and EI) in the enzyme. We model the reaction in the wild type and the D142N mutant. We model multiple conformations taken from

molecular dynamics simulations and model the reaction using well-tested, reliable approaches: adiabatic mapping calculations with high-level energy corrections (using hybrid density functional theory).[36−38] Only the first step (glycosylation) of ChiB was modeled here. Although the rate-limiting step of ChiB is not certain,[6,18,39] this glycosylation step is important in GHs.[5,40,41] The reaction mechanism of the D142N mutant was also investigated here. To the best of our knowledge, this is the first molecular modeling study of the substrate-assisted mechanism of GH18 chitinases. The findings may also apply to other related GH families (GH20, GH56, GH84, and GH85) believed to utilize the substrate-assisted catalytic mechanism.

MATERIALS AND METHODS

Preparation of Wild-Type and D142N Mutant Enzyme−Substrate Complexes. The initial structure of the enzyme−substrate complex was built from the crystal structure [PDB[42] entry 1E6N[6]) of an inactive E144Q ChiB from *S. marcescens* in complex with the substrate penta-*N*-acetyl-chitopentaos (NAG_5), as shown in Figure 1. Gln144 was mutated (in silico) back to glutamate to generate a wild-type structure on the basis of the crystallographic coordinates of glutamine (Q144). The D142N mutant structure was built on the basis of the resulting wild-type structure via replacement of residue Asp142 with Asn142. Note that a rotamer of Asn142 was chosen on the basis of the H-bonding pattern observed in the crystal structure of the D142N mutant[35] in which the carbonyl oxygen of Asn142 formed a hydrogen bond with the HN atom of the acetamido group and the amino group (NH_2) pointed toward Glu144 (see Table 5). All crystallographic water molecules were kept. Hydrogen atoms that are not observed in the crystal structure were added onto the resulting structures of the wild type and mutant (including the crystallographic water molecules), using the HBUILD subroutine in CHARMM.[43] The protonation states of all ionizable amino acid residues were assigned on the basis of the pK_a estimated via PROPKA version 2.0 (http://propka.ki.ku.dk)[44] at their physiological pH values. Aspartate and glutamate residues were deprotonated, with the exception of the catalytic acid/base (Glu144) and Asp142, which were protonated, consistent with the proposed glycosylation mechanism.[6] Histidine residues (none of which are located near the active site) were modeled in their neutral states; their tautomeric state was assigned on the basis of hydrogen bonding using WHATIF (http://swift.cmbi.ru.nl).[45]

NAG (MM) Parameters. CHARMM22 parameters for the NAG monomer were based on glucose parameters developed by Liang and Brady[46] based on CHARMM22 nucleic acid parameters.[47] The anomeric carbon atom (C1) was defined as their atom type CBS.[48] Additional parameters (see Table S2 of the Supporting Information) were developed[9] for the *N*-acetyl side chain by fitting to ab initio data [at the HF/6-31G(d) level][49] for rotation of this group in 2-*N*-acetyl-pyran. These parameters have been used successfully previously in simulations of hen egg white lysozyme complexes.[9]

Molecular Dynamics (MD) Simulations. All MD simulations were performed using CHARMM[50] (versions c27b2 and c29b2). Protein parameters were taken from the CHARMM22 force field,[46] while additional MM parameters for the NAG substrate were developed in our group as noted above (and in the Supporting Information). The system was prepared for simulations using procedures applied successfully in QM/MM simulations of other enzymes.[9,38,51,52] The enzyme−substrate complex was solvated by a 25 Å radius sphere of CHARMM TIPS3P water molecules[46,53] centered on the anomeric C1 atom (see Figure 2B for atom numbering and some structural parameters used here). A spherical deformable boundary potential[54] with a 25 Å radius was used to prevent the water from "evaporating" from the system. All atoms outside a 25 Å sphere centered on the anomeric carbon (C1) were deleted, while protein heavy atoms in the buffer zone (21−25 Å) were subjected to Langevin dynamics with positional restraints using force constants scaled to increase from the inside to the outside of the buffer. All atoms within 21 Å of the reaction zone were subjected to Newtonian dynamics with no positional restraints. The wild-type system and the D142N system were equilibrated by 280 ps of stochastic boundary molecular dynamics, following the procedure described in refs 38 and 52. An integration time step of 1 fs was used, with all of the bonds involving hydrogen atoms constrained using SHAKE.[55] A restraint (with a small harmonic force constant of 10 kcal mol^{-1} $Å^{-2}$) was applied between the hydroxyl group of Asp142 and the carboxylate oxygen of Glu144 of the wild-type system (see Figure 2A) to maintain the hydrogen bond found in the initial structure, because in unrestrained simulations, the Glu144 side chain tended to rotate

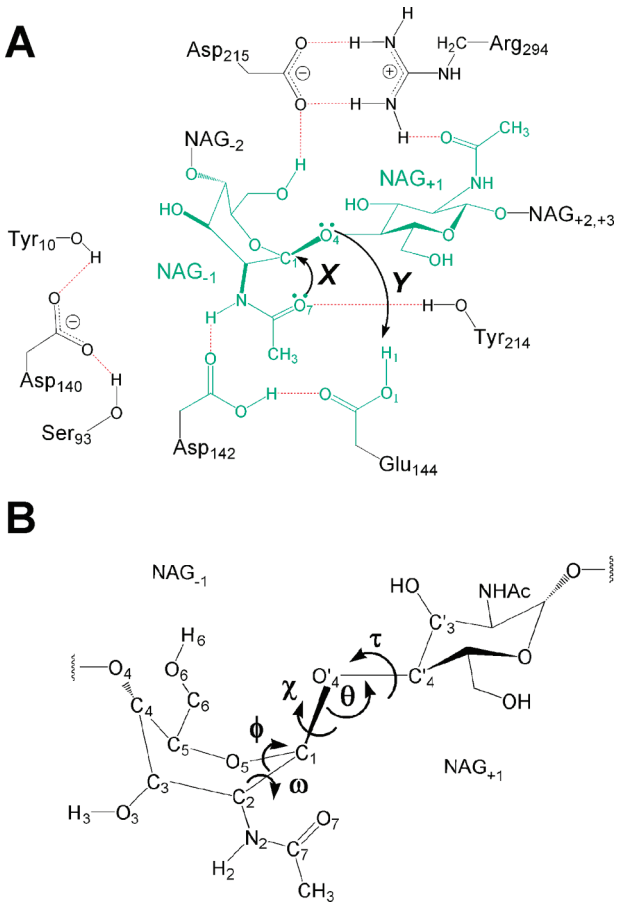

Figure 2. (A) Schematic representation of the QM region containing 73 atoms (green) which are used in the QM/MM calculations and corresponding hydrogen bonds (red) formed by the conserved residues within the active site of ChiB. Individual process (X and Y) involving the glycosylation step of the substrate-assisted mechanism of ChiB is also indicated. (B) Atom numbering of NAG and definitions of some angles monitored in this work.

toward the solvent (see Figures S1 and S2 of the Supporting Information). The same force constant was also applied for the mutant, between the amino group of Asn142 and the carbonyl oxygen of Glu144, to ensure that Asn142 remained in position for reaction.

The MD simulations were used to generate structures for modeling of the reaction, to test effects of active site conformational variability,[56,57] and to investigate the interactions and test the stability of the NAG_5 and comparison with the conformations observed in the X-ray structure (chair conformation in subsites −2, −1, 2, and 3 and boat conformation in subsite −1). Four structures ("snapshots") of the wild-type system and the mutant system were taken at 50 ps intervals from the last 250 ps of the MD simulations (from 130 to 280 ps MM/MD simulation); these structures should represent a reasonably diverse set of enzyme−substrate conformations. The (MM) energy of each of the four snapshots was minimized by the Adopted Basis Newton−Raphson (ABNR) method until the gradient was less than 0.01 kcal mol^{-1} $Å^{-1}$ and then used as a starting point for QM/MM calculations.

QM/MM Potential Energy Surface (PES) Calculations. Each of the four structures for each system was optimized at the QM/MM level [two different semiempirical QM methods were tested (see below)], following the MM optimization described above. Two semiempirical methods, AM1[58] and PM3CARB1,[59] were used for the QM region, to test their suitability. The PM3CARB1 method is a modified version of the PM3 Hamiltonian, which is specifically optimized for carbohydrate modeling.[59,60] The same MM-optimized structures were used in each case, allowing a direct comparison of the two QM/MM methods. In the QM/MM calculations, the system was partitioned into QM and MM regions. The QM region here consists of chitobiose [i.e., NAG_2, the NAG residues in subsites −1 and 1 (see Figure 2A)] of the penta-*N*-acetylchitopentaose substrate, and the side chain atoms of Asp142 and Glu144. This leads to a neutral charge, with 73 QM atoms including four "QQ" link atoms[61,62] to represent four bonds crossing the QM/MM boundary. The remainder of the system [7629 water, protein, and substrate (NAG residues in subsites −2, 2, and 3) atoms] was described by the CHARMM22 force field,[46] including additional parameters for the NAG monomer as described above. We also performed separate calculations with Asp142 or Asn142 treated with MM, to investigate the role of Asp142 in electrostatic stabilization.[6,18,19]

The choice of reaction coordinate (RC) is an important step in generating reliable PESs for chemical reactions in QM/MM calculations; it depends on the nature and complexity of the particular reaction.[63] We found that the first reaction step of ChiB involves two distinct processes, proton transfer and nucleophilic attack (see Scheme 1 and Figure 2A). Test calculations of one-dimensional potential energy profiles at the AM1-CHARMM22 and PM3CARB1-CHARMM22 levels, with B3LYP energy corrections using a one-dimensional reaction coordinate ($d[C_1O_4] - d[C_1O_7] + d[O_1H_1] - d[H_1O_4]$), overestimated the reaction barrier (by more than 3 kcal mol^{-1}) compared to two-dimensional potential energy surfaces (i.e., energy calculated as a function of two separate reaction coordinates[57,64]). Thus, two-dimensional potential energy surfaces were calculated here, as applied successfully previously to other enzymes.[36,37,62,64]

Two-dimensional potential energy surfaces were calculated using an adiabatic mapping approach[65] for each of the four structures. The reaction was described by two coordinates (R_X and R_Y) to represent the key steps of the formation of the proposed oxazolinium ion intermediate in the first reaction step (see Figure 2A), i.e., protonation of the glycosidic linkage oxygen (O4) atom by Glu144 (proton H1) (*Y*) and nucleophilic attack on the anomeric carbon (C1) atom by the carbonyl moiety (O7) of the acetamido group of the substrate NAG residue in subsite −1 (*X*). R_X was defined as the difference between two interatomic distances ($R_X = d[C_1O_4] - d[C_1O_7]$) and represents event *X*. R_Y, defined as $d[O_1H_1] - d[H_1O_4]$, describes event *Y*. R_X and R_Y were increased successively in steps of 0.2 and 0.1 Å, respectively, with harmonic restraints of 5000 kcal mol^{-1} $Å^{-2}$. Geometry optimization of the structures was performed at each point until the energy gradient was less than 0.01 kcal mol^{-1} $Å^{-1}$. The energy was then computed by a single-point calculation, removing the energy contributions due to reaction coordinate restraints. Twelve PESs of the wild-type system (eight PESs for AM1-CHARMM22 and PM3CARB1-CHARMM22) and the D142N mutant system (four PESs for AM1-CHARMM22 only) were generated altogether. Semiempirical QM methods are often inaccurate for reaction energies and barriers, so higher-level energy corrections[36] [at the B3LYP/6-31+G(d) DFT level] were performed, as described previously for other enzymes:[36−38,52,66,67] the QM atoms of each structure were isolated, and single-point energy calculations (~300 points per surface, almost 3600 in total) were performed at AM1 or PM3CARB1 and B3LYP/6-31+G(d) levels. The corrected PESs were obtained by subtracting the AM1 or PM3CARB1 energy of the isolated QM region from the total QM/MM energy and adding the B3LYP energy.

RESULTS AND DISCUSSION

Comparison of AM1 and PM3CARB1 Results. AM1 and PM3CARB1 QM/MM calculations were compared in terms of the structure of the enzyme−substrate (ES) complex, the shape and geometry of the potential energy surface, and the reaction barrier. Table 1 lists the structural parameters (e.g., distances, angles, and dihedral angles) for the four QM/MM-optimized structures of the enzyme−substrate (ES) complex calculated at AM1-CHARMM22 and PM3CARB1-CHARMM22 levels in comparison with those of the available X-ray structure of the ES complex of E144Q ChiB (PDB entry 1E6N).

Crystal structures show the NAG sugar in subsite −1 distorted to a boat conformation; this is thought to promote glycosidic bond hydrolysis.[6] An initial test of modeling methods for ChiB is how well they reproduce this boat conformation in subsite −1. The conformation of this NAG ring and its neighboring sugar in subsite 1 can be monitored by measuring the C2(−1)−C1(−1)−O5(−1)−C5(−1) dihedral angle and other structural parameters (e.g., C1−O4 distance and C1−O4−C4 angle) around the glycosidic bond (see Table 1 and Figure 2B). AM1 gave structures in better agreement with experiment than PM3CARB1. AM1-CHARMM22 optimized structures reproduced the boat conformation of the sugar in subsite −1 well: the average C2(−1)−C1(−1)−O5(−1)−C5(−1) dihedral angle was 31.9 ± 1.8°, in good agreement with the crystallographic finding (31.7°), whereas PM3CARB1-CHARMM22-optimized structures exhibited ~5° smaller values of this dihedral angle (Table 1). The NAG residues in all the other subsites (e.g., −2, 1, 2, and 3) remained in the chair conformation (approximately −60.8° to −64.2°), in agreement with the crystal structure. The AM1-CHARMM22-optimized structures gave a better description of the glycosidic bond between the sugar −1 and 1 than PM3CARB1-CHARMM22: AM1-CHARMM22-optimized average distances for C1−O4 and O4−C4 bonds of 1.42 and 1.43 Å, respectively, are reasonably comparable to the experimental values of

Table 1. Structural Parameters (interatomic distances, angles, and dihedral angles, and mean values) of QM/MM-Optimized Structures of the Enzyme−Substrate (ES) Complex at AM1-CHARMM22 and PM3CARB1-CHARMM22 Levels for Four Configurations Modeled from Structures (snapshots) Sampled at 130, 180, 230, and 280 ps of the MD Simulation of Wild-Type ChiB

		AM1					PM3CARB1				
	X-ray[a]	130 ps	180 ps	230 ps	280 ps	mean	130 ps	180 ps	230 ps	280 ps	mean
distance (Å)											
C1−O4′	1.39	1.42	1.43	1.42	1.42	1.42 ± 0.00	1.42	1.42	1.41	1.41	1.42 ± 0.01
O4′−C4′	1.43	1.43	1.43	1.43	1.43	1.43 ± 0.00	1.40	1.40	1.39	1.39	1.39 ± 0.01
C1−O7	2.98	2.92	3.08	3.00	2.98	3.00 ± 0.07	2.96	3.04	3.02	3.03	3.01 ± 0.04
OD2(Asp142)···OE1(Glu144)	2.71[b]	2.81	2.83	2.85	2.82	2.83 ± 0.02	2.80	2.78	2.80	2.78	2.79 ± 0.01
OD1(Asp142)···N2	2.89[c]	3.03	3.06	3.07	3.04	3.05 ± 0.02	3.31	3.42	3.44	3.41	3.40 ± 0.06
OE2(Glu144)···O4′	3.19[c]	3.05	3.05	3.10	3.07	3.07 ± 0.02	2.92	3.45	3.48	3.43	3.32 ± 0.27
OH(Tyr214)···O7	2.66[b]	2.80	2.83	2.82	2.79	2.81 ± 0.02	2.74	2.74	2.75	2.73	2.74 ± 0.01
OD2(Asp215)···O6	2.64[b]	2.75	2.81	2.76	2.83	2.79 ± 0.04	2.68	2.73	2.73	2.74	2.72 ± 0.03
NH2(Arg294)···O7′	3.09[c]	2.85	2.82	2.81	2.81	2.82 ± 0.02	2.78	2.74	2.80	2.75	2.77 ± 0.03
angle (deg)											
C1−O4′−C4′ (θ)	119.6	118.2	119.1	118.2	118.1	118.4 ± 0.5	122.6	124.0	123.9	124.1	123.7 ± 0.7
C2−C1−O4′−C4′ (χ)	−161.1	−161.5	−160.8	−159.5	−160.8	−160.7 ± 0.8	−157.1	−164.3	−158.7	−162.5	−160.7 ± 3.3
C1−O4′−C4′−C3′ (τ)	146.6	149.6	148.3	150.3	149.6	149.5 ± 0.8	135.1	139.2	136.9	137.2	137.1 ± 1.7
C2−C1−O5−C5 (ϕ)	31.7	29.8	34.2	32.1	31.3	31.9 ± 1.8	23.7	30.2	26.3	26.2	26.6 ± 2.7
C3−C2−C1−O5 (ω)	−41.0	−44.9	−45.6	−45.3	−45.4	−45.3 ± 0.3	−36.8	−41.8	−37.5	−38.0	−38.5 ± 2.2
C2′−C1′−O5′−C5′	−64.8	−61.1	−67.7	−64.7	−63.1	−64.2 ± 2.8	−62.2	−64.6	−65.3	−63.8	−64.0 ± 1.3

[a] Values taken from the experimentally determined X-ray structure of E144Q mutant ChiB (PDB entry 1E6N, chain A) from ref 6. [b] O−O distance. [c] N−O distance.

1.39 and 1.43 Å, respectively. On the other hand, for the PM3CARB1-CHARMM22-optimized structure, the average O4−C4 distance (1.39 Å) is shorter than the average C1−O4 distance (1.42 Å) (Table 1). The average angle around the glycosidic bond [C1(−1)−O4(+1)−C4(+1)] from AM1 is 118.4 ± 0.5°, similar to the experimental value of 119.6°, whereas the average angle from PM3CARB1 is notably larger (123.7 ± 0.7°). Similarly, the average C1(−1)−O4(+1)−C4(+1)−C3(+1) dihedral angle from AM1 (149.5 ± 0.8°) is closer to the experimental value (146.6°) than that from PM3CARB1 (137.1 ± 1.7°).

The sugar residues in subsites −1 and +1 (which are included in the QM region) form hydrogen bonds with Asp142, Glu144, Tyr214, Asp215, and Arg294 (Table 1). Hydrogen bond distances between Asp142 and Glu144 and the substrate, and some others in the active site [OD2(Asp142)···N2(−1), OE2(Glu144)···O4(+1), and OD1(Asp142)···OE1(Glu144) distances], are generally quite different (∼0.3−0.4 Å) between the AM1-CHARMM22- and PM3CARB1-CHARMM22-optimized structures (Table 1), except the OD1(Asp142)···OE1(Glu144) distance. Overall, AM1-CHARMM22 better describes the key OD2(Asp142)···N2(−1) and OE2(Glu144)···O4(+1) hydrogen bond distances than PM3CARB1-CHARMM22 (3.40 ± 0.06 and 3.32 ± 0.27 Å, respectively), with values of 3.05 ± 0.02 and 3.07 ± 0.02 Å, respectively, closer to the experimental values (2.89 and 3.19 Å, respectively). Overall, the AM1-CHARMM22 method gives enzyme−substrate (ES) complex structures more consistent with the crystallographic structure (of the mutant ChiB).

Two-dimensional potential energy surfaces (PESs) for the first step of the reaction mechanism of ChiB were generated from the QM/MM-optimized enzyme−substrate complex structures with both semiempirical methods (AM1 and PM3CARB1; low-level surfaces) for the four different configurations of the ES complex. High-level PESs, including energy correction with B3LYP, are denoted as B3LYP/6-31+G(d)//AM1-CHARMM22 and B3LYP/6-31+G(d)//PM3CARB1-CHARMM22. The reaction proceeds through the transition state (TS) structure(s) corresponding to the saddle point(s) on the PES that separates the Michaelis complex (ES) from the intermediate (EI). The low-level PESs with both semiempirical QM/MM methods are similar in shape and geometry. All these PESs have two saddle points, suggesting a stepwise mechanism at these levels of theory. The QM/MM energy of the intermediate (EI) relative to the reactant was significantly higher in the AM1-CHARMM22 PESs than in the PM3CARB1-CHARMM22 PESs (Figure S3 of the Supporting Information). The high-level PESs have clearly different shapes depending on which of the two semiempirical methods was used for geometry optimization, indicating different reaction paths (Supporting Information). B3LYP/6-31+G(d)//AM1-CHARMM22 PESs show only one saddle point, indicating that the transfer of a proton from Glu144 to glycosidic oxygen is concerted with fission of the glycosidic bond (including cyclization of the oxazoline). In contrast, the B3LYP/6-31+G(d)//PM3CARB1-CHARMM22 PESs all have two saddle points, suggesting a stepwise reaction in which the fission of the glycosidic bond and the formation of oxazoline would occur as a first step, followed by the transfer of a proton from Glu144 to the glycosidic oxygen. The AM1-CHARMM22 method appears to be more consistent with experiment, for the reasons discussed above and below. Details of important structures on these B3LYP/6-31+G(d)//AM1-CHARMM22 PESs are described below.

The energy barrier from QM/MM calculations can be compared to the activation free energy derived from experimental kinetics using transition state theory.[68,69] The activation free energy of ChiB is ∼16.1 kcal mol^{-1} (Table 2), estimated from the experimental rate constant (k_{cat}) of 28 s^{-1} at 310 K.[39] All the PESs show only a small variation in the barrier between the different surfaces at a given level of theory: a variation of ∼3−4 kcal mol^{-1}. At the B3LYP/6-31+G(d)//AM1-CHARMM22 level, the barriers ranged from 15.8 to 19.8 kcal mol^{-1} (Table 2). The B3LYP/6-31+G(d)//PM3CARB1-CHARMM22 barriers are higher [20.1−23.3 kcal mol^{-1} (Table S2 of the Supporting Information)] but show a similar variability. These results indicate that structural fluctuations of the ChiB−NAG_5 complex do not significantly affect the reaction barrier. There is, however, a significant difference in the

dx.doi.org/10.1021/bi101362g |Biochemistry 2011, 50, 4697–4711

Table 2. QM/MM Energies (left) and Stabilization Energies (right) in Kilocalories per Mole Relative to the Energy of the Reactant (ES) along the Crucial Species [transition state (TS), $^4C_1$-chair intermediate (EI1), and $B_{3,O}$-boat intermediate (EI2)] for the Wild-Type and D142N Mutant Complexes (sampled from MD simulations at 130, 180, 230, and 280 ps) of ChiB[a]

	QM/MM energy				stabilization energy[b]			
snapshot	TS	EI1(chair)	EI2(boat)	ΔEI[c]	TS	EI1(chair)	EI2(boat)	ΔEI[c]
wild type								
130 ps	16.3	−11.8	−12.3	0.5	2.7	25.1	28.7	3.6
180 ps	15.8	−9.5	−11.8	2.3	5.0	22.4	23.5	1.1
230 ps	19.8	−4.2	−5.1	0.9	0.3	18.9	25.3	6.4
280 ps	19.2	−11.4	−12.8	1.4	−0.2	24.8	28.5	3.7
mean	17.8 ± 2.0	−9.2 ± 3.5	−10.5 ± 3.6	1.3 ± 0.8	2.0 ± 2.4	22.8 ± 2.9	26.5 ± 2.5	3.7 ± 2.2
expt	16.1[d]							
D142N								
130 ps	19.5	−10.0	−10.4	0.4	0.2	23.1	26.3	3.2
180 ps	20.9	−1.2	−0.1	1.1	−0.6	15.3	16.0	0.7
230 ps	21.1	−8.1	1.0	9.1	−1.1	18.6	17.3	1.3
280 ps	16.0	−11.2	−6.6	4.6	3.4	24.0	23.0	1.0
mean	−7.6 ± 4.5	−4.0 ± 5.4	0.5 ± 2.0	20.3 ± 4.1	20.7 ± 4.8	1.6 ± 1.1		
expt	19.0[e]							

[a] Note that the modeled pH value for both model systems was 7.0. [b] Stabilization energies calculated by subtracting the QM energies (in the gas phase) from QM/MM energies relative to the energy of the reactant (ES). [c] ΔEI = EI1 − EI2. [d] Estimated from the ChiB activity with a natural substrate at pH 6.1 and 37 °C from ref 39. [e] Estimated from the ChiB activity with an artificial substrate (4MU-NAG$_2$) at pH 6.3 and 37 °C from ref 18.

energy barrier between the PESs calculated with the different QM methods. The difference in energy barriers between the two methods is approximately 4−5 kcal mol^{-1}. The B3LYP/6-31+G(d)//AM1-CHARMM22 barriers (15.8−19.8 kcal mol^{-1}) are significantly lower and closer to the experimental value than the B3LYP/6-31+G(d)//PM3CARB1-CHARMM22 barriers (20.1−23.3 kcal mol^{-1}). Combined with the poorer modeling of the enzyme−substrate complex with the latter method, this provides a good indication that the B3LYP/6-31+G(d)//AM1-CHARMM22 results are preferable, being more consistent with experiment, and provide a good method for modeling this reaction. The AM1-CHARMM22 method with B3LYP correction was thus chosen for calculation of the potential energy surface for the reaction in the wild-type and D142N mutant enzymes. The PM3CARB1 QM/MM results are given as Supporting Information for comparison. The B3LYP/6-31+G(d)//AM1-CHARMM22 results are the focus of the discussion below.

Reaction Path and Mechanism. The B3LYP/6-31+G(d)//AM1-CHARMM22 PESs are shown in Figure 3 as contour plots, along with the corresponding structural changes of the NAG residue in subsite −1. The energies given are the total QM/MM energies in kilocalories per mole relative to the reactant complex (ES). Important points on the PESs are the Michaelis (substrate) complex (ES), transition state (TS), and intermediates (EI1 and EI2). These are apparent on the wild-type and D142N PESs (see Figure 3): both show the pathway (ES → TS → EI1 → EI2) and similar conformational changes of the sugar at subsite −1 for all surfaces. The lowest-energy path in all cases goes approximately diagonally through the middle of the PESs at the TS (approximate saddle point is found at $R_X \sim -0.2$ Å and $R_Y \sim -0.5$ Å) and then to the EI2 (at $R_X \sim 1.6$ Å and $R_Y \sim -0.5$ Å). The PESs also show two minima (EI1 and EI2) with significantly different energies and the sugar (−1) conformations for both the wild type and the D142N mutant (see the discussion below). These reaction paths indicate that the transfer of a proton from Glu144 is concerted with the breaking of the scissile glycosidic bond and the cyclization of the oxazolinium ion intermediate. The results here indicate that the breaking of the scissile glycosidic bond directly involves the assistance of the acetamido group, which facilitates the departure of the leaving group by attacking at the anomeric center.

Energetics and Structures along the Reaction Path. The B3LYP/6-31+G(d)//AM1-CHARMM22 energies from four different QM/MM PESs for the crucial species (TS, EI1, and EI2) in the wild type and the D142N mutant are summarized in Table 2. These QM/MM energies are the (total) energies of the various structures relative to the reactants; thus, the energy of the transition state structure gives the energy barrier to reaction. The average calculated barriers of the wild type and D142N are 17.8 ± 2.0 and 19.4 ± 2.4 kcal mol^{-1}, respectively, which are in good agreement with the experimental barriers of 16.1 and 19.0 kcal mol^{-1}, respectively. It is important to stress that the experimental activation energy for the mutant (D142N) is derived from experimental data obtained with an artificial substrate (often termed 4MU-NAG$_2$); i.e., the leaving group is not a sugar molecule.[18] The k_{cat} values for a sugar leaving group and a 4MU leaving group are similar;[39] we therefore compare this value here in our calculations for the mutant enzyme. Another factor to consider in comparing with the experiment (particularly for the mutant) is the possible effect of pH; there does not appear to be a large change in pH dependence caused by the mutation in this case.[18]

Both the wild type and the D142N mutant show relatively stable intermediates. Both EI1 and EI2 have significantly lower energies (Table 2) than the reactant (ES), in the wild type and in the mutant. A notable difference between the wild type and the mutant is that the boat conformation of the intermediate (EI2) is in all cases more stable than the chair (EI1), whereas for the mutant, the chair conformation is more stable in most cases (three of four). Stabilization energies are also listed in Table 2;

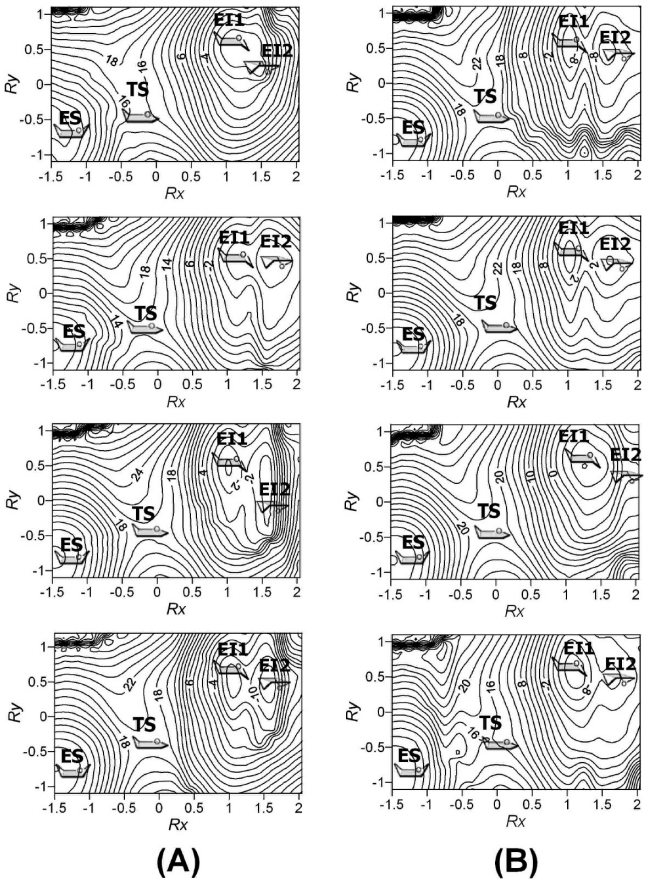

Figure 3. Contour plots of the B3LYP/6-31+G(d)//AM1-CHARMM22 QM/MM potential energy surfaces of the glycosylation step of the wildtype (A) and D142N mutant (B) ChiB.

this stabilization energy gives the stabilization of each species by the enzyme, relative to the stabilization of the reactants, indicating the amount of stabilization provided by the enzyme during the reaction. As shown in Table 2, both the wild type and the D142N mutant show large stabilization energies for the intermediate. The stabilization energy of the intermediate is significantly higher than that of the TS. The average values of the stabilization energies are 22.8 ± 2.9 kcal mol^{-1} at EI1 and 26.5 ± 2.5 kcal mol^{-1} at EI2 (wild type) and 20.3 ± 4.1 kcal mol^{-1} at EI1 and 20.7 ± 4.8 kcal mol^{-1} at EI2 (D142N mutant) (Table 2). This shows an important role of the enzyme in effectively stabilizing the oxazolinium ion intermediate. These results also suggest that the intermediate (particularly the EI2 form) is better stabilized in the wild type than in the D142N mutant.

Representative structures of ES, TS, EI1, and EI2 from the B3LYP/6-31+G(d)//AM1-CHARMM22 PES calculated for the 280 ps snapshot are shown in Figure 4. Structural parameters averaged over the four structures of the crucial species (ES, TS, EI1, and EI2) are listed in Table 3. Only the structures of the wild type are shown because the D142N mutant also gave similar structures (Table 3). The reactant (ES) structure is shown in Figure 4A. Here, the protonated Glu144 forms a hydrogen bond to the glycosidic oxygen atom (O4) with an average O4′−HE2(Glu144) distance of 1.77 Å in the wild type, which is significantly shorter than that in the mutant (1.83 Å). The average OE1(Glu144)−HD(Asp142) distance (2.05 Å) of the wild type is shorter than the average OE1(Glu144)−HD(Asn142) distance (2.14 Å) of the mutant. The sugar ring in subsite −1 in the reactant remains in the boat ($^{1,4}B$) conformation ($\phi \sim 18°$, and $\omega \sim -30°$) for both the wild type and the mutant, similar to the experiment [$\phi = 31.7°$, and $\omega = -41°$ (Table 1)]. The NAG residues in the other subsites (−2, 1, 2, and 3) remain in the chair ($^4C_1$) conformation (data not shown). Figure 4A also show hydrogen bonds formed between the NAG residues in subsites −1 and 1 (in the QM region) and conserved residues; NAG_{-1} is stabilized by hydrogen bonds from Asp142, Tyr214, and Asp215, while NAG_{+1} forms hydrogen bonds with Glu144 and Arg294. These residues maintain hydrogen bonds with NAG_{-1} and NAG_{+1} throughout the reaction.

In the transition state (TS), the pyranose ring in subsite −1 of both the wild-type and D142N mutant enzymes adopts a conformation in which C2, C1, O5, and C5 are approximately coplanar; the wild-type (−1.9 ± 2.7°) TS is slightly more planar than that in the mutant (−4.3 ± 1.0°). This conformation is approximately a half-chair structure ($^4H_5$) and is closely related to an envelope structure (^4E). The TS structure has oxacarbenium ion-like character, with an sp^2-hybridized anomeric center and delocalized positive charge between the endocyclic ring oxygen (O5) and the anomeric center (C1); the C1−O5 bond at the ES was shortened and became the partial double bond at the TS in both the wild type and the mutant [∼1.40 ± 0.00 Å at the ES to ∼1.35 ± 0.01 Å at the TS (see Table 3)]. The Mulliken charge increases for C1 and O5 from the ES to the TS in both the wild type (C1, 0.146*e* → 0.261*e*; O5, −0.289*e* → −0.199*e*) and the mutant (C1, 0.154*e* → 0.287*e*; O5, −0.290*e* → −0.180*e*) (Tables 4 and 5). It is notable that this TS structure for both the wild type and the mutant has unequal distances of the scissile glycosidic bond (C1−O4′) and the forming distance (C1−O7) of the anomeric carbon (C1) and the *N*-acetyl carbonyl oxygen (O7); the latter is greater than the former (Table 3). Most of the hydrogen bond distances formed by the conserved residues around the NAG at subsites −1 and 1 are shorter than in the reactant (see Figure 4B and Table 3), indicating an important role of these conserved residues in transition state stabilization. The O4′−HE2(Glu144) distance decreases by 0.3−0.4 Å from the reactant to the TS (Table 3).

After the TS, a bicyclic structure of the oxazolinium ion intermediate was initially formed at EI1 by shortening the forming C1−O7 distance of the anomeric carbon (C1) and the *N*-acetyl carbonyl oxygen (O7) to fuse the oxazoline with the pyranose ring (Table 3). At the same time, the conformation of the pyranose ring at subsite −1 was altered from the envelope (^4E) at the TS to chair ($^4C_1$) at EI1, as shown by the change in the C2−C1−O5−C5 dihedral angle (ϕ) from nearly planar to approximately −19.0 ± 2.0° (Table 3). Subsequently, the chair conformation at the EI1 unexpectedly changed to a boat conformation ($B_{3,O}$) at EI2 (Figures 4 and 5), shown, for example, by the planarity of the C3−C2−C1−O5 dihedral angle (ω) in EI2 (Table 3). Note that no transition state structure was observed during the conformational change from EI1 to EI2. The change in the geometry and the position in space of the oxazolinium ion intermediate EI1 results in further rearrangement of its conformation at EI2, perhaps to reduce the ring strain raised from a shortened C1−O7 bond [1.47 ± 0.01 Å in EI1 to 1.43 ± 0.00 Å in EI2 (see Figure 5)]. The oxazolinium cation character of this intermediate state is shown by the change of the Mulliken charge on the N2 atom that is approximately reduced by half on going from the ES to the EI [−0.377*e* at the ES to approximately −0.197*e* and −0.164*e* at EI1 and EI2, respectively (Table 4)] in the wild type. The D142N mutant shows similar trends

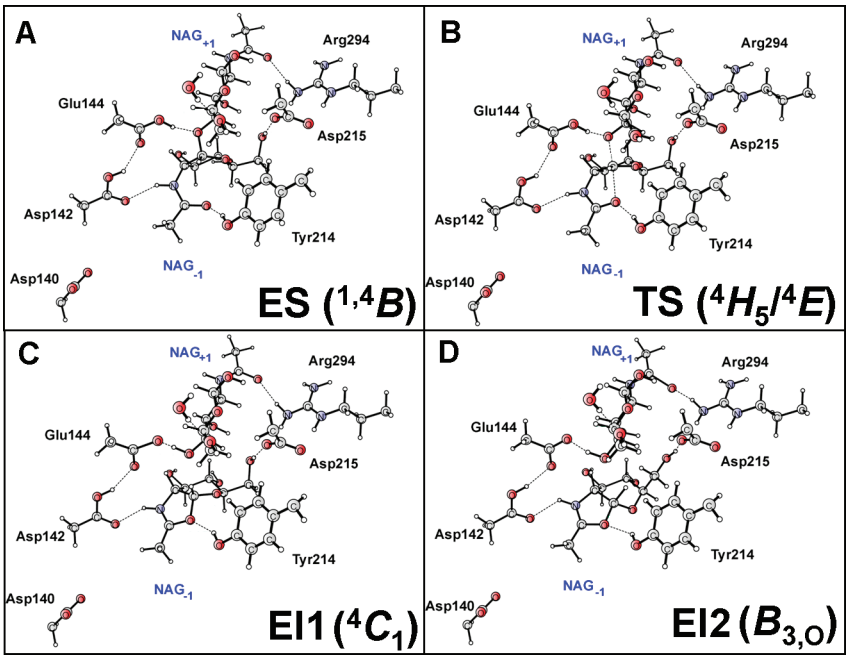

Figure 4. The QM/MM optimized structures of the enzyme-substrate (ES) complex, transition state (TS), and oxazolinium ion intermediates in both ^{4}C1−chair (EI1) and $B_{3,O}$−boat (EI2) conformation [from the B3LYP/6-31+G(d)//AM1-CHARMM22 PES calculated for the 280 ps snapshot]. Residues that formed hydrogen bonds with the QM substrate (NAG_{-1} and NAG_{+1}) are also indicated.

Table 3. Selected Structural Parameters[a] Obtained at the B3LYP/6-31+G(d)//AM1-CHARMM22 Level of Theory for Important Structures along the Glycosylation Path of the Wildtype and D142N Mutant ChiB

	wild type				D142N			
	ES	TS	EI1(chair)	EI2(boat)	ES	TS	EI1(chair)	EI2(boat)
distance (Å)								
C1−O4′	1.43 ± 0.01	1.84 ± 0.05	2.55 ± 0.04	3.01 ± 0.07	1.44 ± 0.01	1.93 ± 0.01	2.56 ± 0.09	3.11 ± 0.09
C1−O5	1.40 ± 0.00	1.35 ± 0.01	1.39 ± 0.00	1.41 ± 0.01	1.40 ± 0.00	1.34 ± 0.01	1.39 ± 0.00	1.41 ± 0.01
C1−O7	3.03 ± 0.08	2.12 ± 0.02	1.47 ± 0.01	1.43 ± 0.00	3.00 ± 0.01	2.10 ± 0.01	1.47 ± 0.01	1.43 ± 0.00
C7−O7	1.25 ± 0.00	1.26 ± 0.01	1.37 ± 0.00	1.38 ± 0.00	1.25 ± 0.00	1.27 ± 0.00	1.37 ± 0.00	1.38 ± 0.00
C7−N2	1.39 ± 0.00	1.38 ± 0.01	1.33 ± 0.00	1.33 ± 0.00	1.38 ± 0.01	1.37 ± 0.00	1.33 ± 0.00	1.33 ± 0.00
H2−OD1(Asp/Asn142)	2.14 ± 0.03	2.05 ± 0.01	2.01 ± 0.02	2.05 ± 0.04	2.13 ± 0.03	2.05 ± 0.02	1.98 ± 0.01	2.05 ± 0.02
O4′−HE2(Glu144)	1.77 ± 0.05	1.46 ± 0.08	1.03 ± 0.01	1.07 ± 0.03	1.83 ± 0.04	1.47 ± 0.01	1.03 ± 0.01	1.04 ± 0.00
O7−HH(Tyr214)	1.89 ± 0.02	1.84 ± 0.01	1.96 ± 0.01	2.06 ± 0.01	1.87 ± 0.01	1.84 ± 0.02	1.95 ± 0.01	2.07 ± 0.03
H6−OD2(Asp215)	1.84 ± 0.04	1.81 ± 0.05	1.81 ± 0.04	1.81 ± 0.04	1.91 ± 0.03	1.85 ± 0.03	1.84 ± 0.01	1.87 ± 0.02
O7′−HH21(Arg294)	1.86 ± 0.02	1.86 ± 0.02	1.86 ± 0.01	1.86 ± 0.03	1.89 ± 0.05	1.87 ± 0.03	1.86 ± 0.01	1.85 ± 0.02
OE1(Glu144)−HD(Asp/Asn142)	2.05 ± 0.01	2.04 ± 0.01	1.96 ± 0.01	1.96 ± 0.02	2.14 ± 0.01	2.11 ± 0.01	2.02 ± 0.02	2.00 ± 0.01
angle (deg)								
C2−C1−O5−C5 (ϕ)	18.2 ± 3.4	−1.9 ± 2.7	−18.7 ± 2.5	56.3 ± 3.3	18.7 ± 2.1	−4.3 ± 1.0	−19.3 ± 2.2	56.1 ± 1.7
C3−C2−C1−O5 (ω)	−30.8 ± 2.5	−10.7 ± 3.2	16.3 ± 3.2	−3.4 ± 5.8	−30.5 ± 2.3	−6.5 ± 1.7	17.9 ± 2.7	−0.5 ± 2.5

[a] Distances and angles averaged over the four configurations (based on the four PESs from snapshots at 130, 180, 230, and 280 ps) and their standard deviations are also given.

(Table 5). A significant difference between the wild type and the mutant can be seen for the OE1(Glu144)−HD(Asp/Asn142) H-bond distance; although trends in the reaction are similar, the wild type has a shorter H-bond distance in all species (Table 3).

Conformational Change of the Pyranosyl Ring along the Glycosylation Path. The structural evolution of the sugar in subsite −1 along the reaction path is shown in Figure 5. The formation of the oxazolinium ion intermediate occurs in association with a bond (C1−O7) distance between the anomeric center (C1) and the carbonyl oxygen (O7) of the 2-acetamido group (from ∼3.00 Å at $^{1,4}B$ to 1.43 Å at $B_{3,O}$). The structural change is as follows: boat ($^{1,4}B$) → half-chair ($^4H_5$)/envelope (^4E) → chair ($^4C_1$) ↔ boat ($B_{3,O}$). This is consistent with the antiperiplanar lone pair hypothesis.[70] On the basis of this hypothesis, the conformational change (from boat at the ground state to envelope at the TS) directs the scissile glycosidic bond to a pseudoaxial, creatng better overlap between the lone pair orbital on the nucleophile (O7) and the bonding and antibonding orbitals

dx.doi.org/10.1021/bi101362g |*Biochemistry* 2011, 50, 4697–4711

(C1−O4) involving the leaving group (see Figure S5 of the Supporting Information). Such electronic reorganization[70] is required for the fission of the glycosidic bond and thus allowed the nucleophilic substitution at the anomeric center.[71] Note that the observed conformational change for the pyranosyl ring in subsite −1 here suggests a conformational pathway different from Stoddart's diagram;[21] a simple interpretation of this could indicate $^{1}S_{3} \rightarrow {}^{4}H_{3} \rightarrow {}^{4}C_{1}$ as a possible conformational route for GH families 18, 20, 56, and 84.[5,20] It should be remembered that Stoddart's diagram describes only the relationships between possible ring conformers of a generic monosaccharide and does not imply that each conformer represents a free energy minimum for any particular sugar ring. Our results indicate that the pyranosyl ring in subsite −1 may have more complicated conformational behavior. The conformation of the sugar may depend on many factors, e.g., protonation state and protein environment.[20] The anomeric effect and, vitally, the tendency to coplanarity of the C3, C2, C1, and O5 pyranose ring atoms induced by the cyclic formation of a five-member ring formed by the *N*-acetamino group are other important factors that could cause different

Table 4. Average Mulliken Charges, in Units of *e* (calculated at the AM1-CHARMM22 level), of Some Important Atoms (see the scheme below for EI; the hydroxyl group of the sugar is not shown for the sake of clarity) of Important Structures along the Glycosylation Path of Wild-Type ChiB

atom	ES	TS	EI1(chair)	EI2(boat)
C1	0.146	0.261	0.127	0.099
N2	−0.377	−0.360	−0.197	−0.164
O4	−0.341	−0.527	−0.461	−0.495
O5	−0.289	−0.199	−0.231	−0.267
C7	0.304	0.298	0.270	0.267
O7	−0.388	−0.426	−0.218	−0.167
O8	−0.393	−0.417	−0.479	−0.468
O9	−0.325	−0.318	−0.309	−0.315
O1	−0.334	−0.391	−0.569	−0.553
O2	−0.422	−0.467	−0.635	−0.621

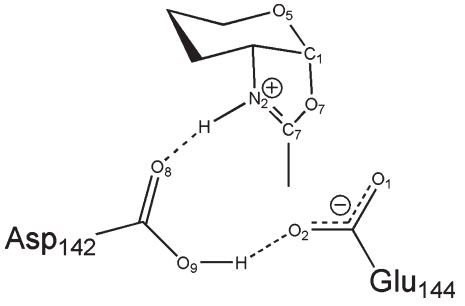

Table 5. Average Mulliken Charges, in Units of *e* (calculated at the AM1-CHARMM22 level) of Some Important Atoms (see the scheme below for EI; the hydroxyl group of the sugar is not shown for the sake of clarity) of Important Structures along the Glycosylation Path of D142N Mutant ChiB

atom	ES	TS	EI1(chair)	EI2(boat)
C1	0.154	0.287	0.120	0.095
N2	−0.379	−0.356	−0.185	−0.161
O4	−0.345	−0.585	−0.452	−0.453
O5	−0.290	−0.180	−0.240	−0.263
C7	0.302	0.299	0.263	0.263
O7	−0.390	−0.431	−0.208	−0.168
O8	−0.412	−0.437	−0.488	−0.481
N3	−0.428	−0.418	−0.407	−0.414
O1	−0.332	−0.387	−0.570	−0.575
O2	−0.399	−0.457	−0.629	−0.625

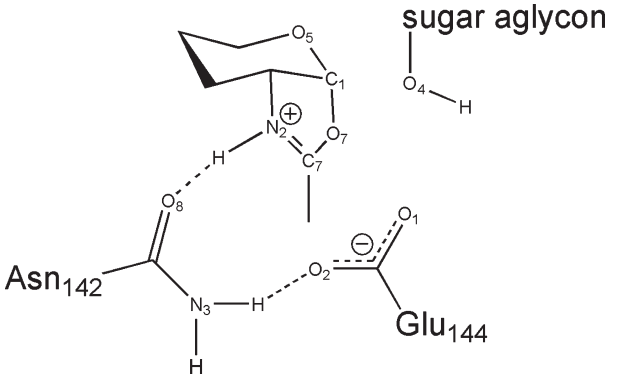

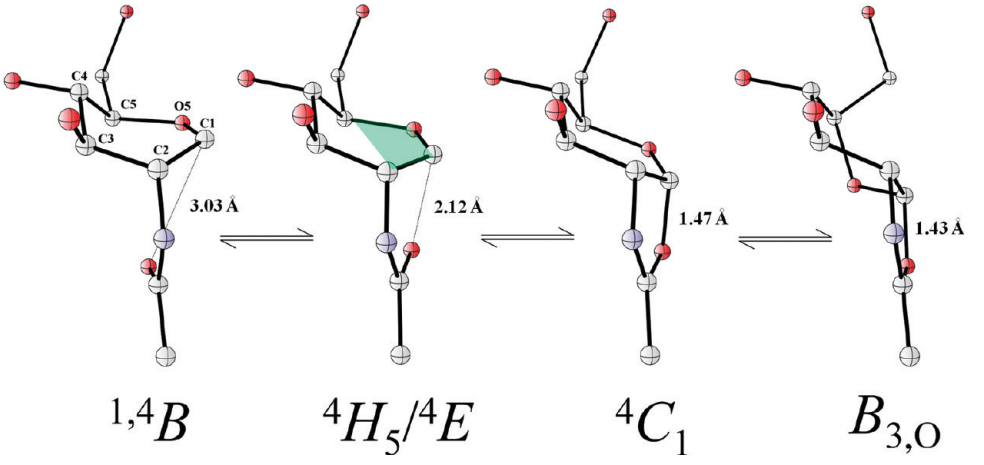

Figure 5. Structural evolution of the pyranosyl ring in subsite −1 along the glycosylation path [from the B3LYP/6-31+G(d)//AM1-CHARMM22 PES based on the 280 ps snapshot].

dx.doi.org/10.1021/bi101362g |*Biochemistry* 2011, 50, 4697–4711

Table 6. $\Delta E(QM/MM_{elec})$ Values, Averaged over Four Configurations, Defined by AM1-CHARMM22 Electrostatic Energy Differences between the Complete Model Structure and the Structure with Each Selected Residue Deleted for Important Structures along the Glycosylation Path of the Wild Type and the D142N Mutant[a]

	wild type				D142N			
residue deleted[b]	ES	TS	EI1(chair)	EI2(boat)	ES	TS	EI1(chair)	EI2(boat)
Gly96−HA2:OE1	3.51	3.23	3.19	2.76	3.84	3.37	3.52	3.21
Trp97−HN:O3	6.06	5.76	5.67	5.48	6.00	5.65	6.15	6.08
Asp140−OD2:HB2	15.43	18.12	39.82	45.38	17.22	21.42	43.39	48.96
Tyr145−OH:O6′	3.19	2.66	1.23	1.33	4.12	3.42	1.33	1.58
Tyr214−OH:O7	6.95	6.45	3.34	2.48	6.64	5.71	2.61	1.27
Asp215−OD2:H6	−31.59	−35.08	−38.20	−37.77	−29.45	−32.63	−35.17	−31.85
Arg294−HH21:O7′	29.98	31.86	41.22	44.32	28.11	30.85	38.41	38.81

[a] ChiB residues with $|\Delta E(QM/MM_{elec})|$ values of >2 kcal mol^{-1} are listed here. Note that the Asp215−Arg294 pair forms a strong salt-bridge. [b] Selected residue deleted and its atom that is interacting with the substrate and residue 142 (or Glu144 (shown in italics)).

Table 7. Changes in the ΔE(QM/MMelec) Stabilization Energies (in kilocalories per mole) for Individual ChiB Residues in Table 6 along the Glycosylation Path from the Enzyme-Substrate (ES) Complex to the Transition State (TS) and the $^4C_1$-Chair Intermediate (EI1) or the $B_{3,O}$-Boat Intermediate (EI2) of the Wildtype and D142N Mutant ChiB[a]

	wild type			D142N		
residue[b]	ES → TS	ES → EI1(chair)	ES → EI2(boat)	ES → TS	ES → EI1(chair)	ES → EI2 (boat)
Gly96−HA2:OE1	−0.28	−0.33	−0.76	−0.46	−0.31	−0.63
Trp97−HN:O3	−0.30	−0.39	−0.58	−0.35	0.15	0.09
Asp140−OD2:HB2	2.70	24.39	29.96	4.20	26.18	31.74
Tyr145−OH:O6′	−0.53	−1.96	−1.86	−0.71	−2.80	−2.55
Tyr214−OH:O7	−0.50	−3.61	−4.47	−0.93	−4.03	−5.37
Asp215−OD2:H6	−3.48	−6.60	−6.17	−3.18	−5.72	−2.41
Arg294−HH21:O7′	1.88	11.24	14.35	2.73	10.29	10.70

[a] Note that the Asp215−Arg294 pair forms a strong salt-bridge. [b] Selected residue deleted and its atom that is interacting with the substrate and residue 142 (or Glu144 (shown in italics)).

conformers of the pyranosyl ring. The AM1 method also has well-known limitations for conformations of carbohydrates. Higher-level QM/MM calculations, with structure optimization at ab initio or DFT levels,[69,72,73] will be useful in exploring these questions in the future.

Contributions of Residues to Electrostatic Stabilization. Analysis of the interaction of the reacting system with the protein environment can identify key groups involved in stabilizing transition states and intermediates in enzymes.[36,38,52,74] The interaction energies of protein residues in the environment (treated by molecular mechanics) with the reacting system (treated by quantum mechanics) are calculated for each of the crucial species in the reaction (here ES, TS, EI1, and EI2). Residues that significantly stabilize the TS or EI relative to the ES are predicted to have a significant effect on the reaction. This method can identify catalytically important interactions.[75,76] For the wild type and the D142N mutant, the QM/MM interaction energy for each complex with and without each selected residue deleted was evaluated.[38] Electrostatic stabilization by any individual residue of more than 2 kcal mol^{-1} is summarized in Table 6. A positive and negative value of $\Delta E(QM/MM_{elec})$ indicates that the residue stabilizes or destabilizes the reacting system, respectively.

The same residues are important in both the wild type and the D142N mutant, with similar trends of QM/MM electrostatic energies but different amounts, particularly for charged residues. Those amino acid residues with $|\Delta E(QM/MM_{elec})|$ values of >2 kcal mol^{-1} are Gly96, Trp97, Asp140, Tyr145, Tyr214, Asp215, and Arg294. If Asp215 is excluded, the six other residues all provide the stabilization to the four critical structures (ES, TS, EI1, and EI2) (Table 6). Charged residues (i.e., Asp140, Asp215, and Arg294) play an important role in electrostatic stabilization of the wild type and the mutant ChiB, as evidenced by a large electrostatic contribution $[|\Delta E(QM/MM_{elec})| > 15$ kcal mol^{-1} (Table 6)] along the reaction path. Asp140 and Arg294 stabilize the key species in the following order: ES < TS < EI. Most other residues in the D142N mutant stabilize the same crucial species in the reverse order (ES > TS > EI).

To improve our understanding of the key residues that have a significant effect in the reaction, the changes in the (electrostatic) stabilization energies ($\Delta\Delta E$) were calculated for the residues in Table 6 in both the wild type and the mutant, and the results are listed in Table 7. Similar stabilization energies are observed in the intermediate of both the wild type and the mutant. The residues with $|\Delta\Delta E|$ values of >2 kcal mol^{-1} in the wild type and the D142N enzyme are Asp140, Tyr145, Tyr214, Asp215, and Arg294. Asp140 and Arg294 are still the main contributors to the electrostatic stabilization of the intermediate, and some stabilization to the transition state. More importantly, Asp140, which is quite far from the QM residues and the oxazolinium ion, provides significant electrostatic stabilization, particularly to the EI, suggesting that this residue is important not only in substrate binding[6,18] but also in catalysis (see below). A decrease in the levele of stabilization from the reactant to the intermediate, shown by negative values, is found for Tyr145,

dx.doi.org/10.1021/bi101362g |*Biochemistry* 2011, 50, 4697–4711

Table 8. Average Stabilization Energies [ΔE(QM/MM$_{elec}$), i.e., electrostatic] for Residues Asp142 and Asn142 of the Wild Type and the D142N Mutant, Respectively[a]

	ΔE(QM/MM$_{elec}$)				$\Delta\Delta E$(QM/MM$_{elec}$)		
residue	ES	TS	EI1	EI2	ES → TS	ES → EI1	ES → EI2
Asp142	5.7	11.9	21.1	19.4	6.2	15.4	13.7
Asn142	2.8	6.2	17.2	15.3	3.4	14.4	12.5

[a] Important structures along the glycosylation path (left-hand side) and a corresponding change in stabilization energy [$\Delta\Delta E$(QM/MM$_{elec}$)], showing significant increases in the levels of stabilization during the reaction (right-hand side).

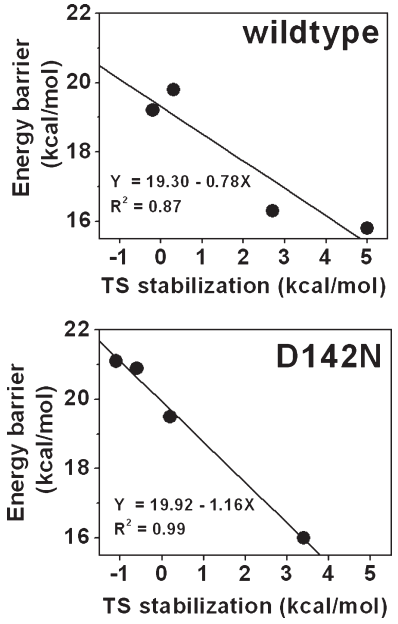

Figure 6. Plot of energy barrier vs the transition state (TS) stabilization energy for the four structures (each) of the wild type and the D142N mutant, calculated at the B3LYP/6-31+G(d)//AM1-CHARMM22 level.

Tyr214, and Asp215 (Table 7); this destabilization is pronounced in the intermediate.

Role of Asp142 in Electrostatic Stabilization of the Transition State and Intermediate. To investigate the role of Asp142 in stabilizing the transition state, the intermediate, or both, we calculated electrostatic contributions to stabilization provided by Asp142 or Asn142 (treated here by molecular mechanics). Asp142 and Asn142 for the wild type and the D142N mutant, respectively, both stabilize the crucial species in the following order: ES < TS < EI; i.e., they provide stronger stabilization to the intermediate than to the transition state (Table 8). A significant effect of the D142N mutation is clear in reduced stabilization energies (ΔE) along the reaction path. This weaker stabilization is expected because replacement of Asp142 with asparagine would lead to weaker electrostatic interaction with Glu144 and/or the acetamido group of the substrate. In the reactant and the transition state, the stabilization energies significantly decrease [~2-fold (Table 8)], resulting in a significant 2-fold reduction (from 6.2 to 3.4 kcal mol^{-1}) for the stabilization to the transition state provided by Asp142, which also indicates that the mutation significantly affects the relative stability of the transition state.

A plot of transition state stabilization versus calculated barrier for the four structures of the wild type and the D142N mutant (Figure 6) shows a good linear correlation (R^2 values of 0.87 and 0.99 for the wild type and the mutant, respectively) between the transition state stabilization and the barrier, with slopes of −0.78 and −1.16 for the wild type and the mutant, respectively. This demonstrates the importance of transition state stabilization for efficient reaction in the enzyme. As shown by the stabilization energies calculated above, stabilization of the intermediate is greater, however.

CONCLUSIONS

QM/MM modeling supports the proposal of a substrate-assisted reaction mechanism in retaining GH18 chitinases and suggests interesting conformational changes along the reaction pathway for the formation of the oxazolinium ion intermediate. The energy barriers with good levels of QM are approximately 15.8−19.8 kcal mol^{-1}, in good agreement with the experimental energy barrier of 16.1 kcal mol^{-1} calculated from the experimental rate constant (28 s^{-1} at 310 K[39]). The transfer of a proton from Glu144 to the glycosidic oxygen is concerted with the nucleophilic attack at the anomeric center by the carbonyl oxygen of the *N*-acetamino group. The transition state structure has oxacarbenium ion-like character. The enzyme significantly stabilizes the intermediate. Two stable intermediates with different conformations ($^4C_1$-chair and $B_{3,O}$-boat) were unexpectedly observed. Complex conformational changes were found during the reaction for the glycosyl residue in subsite −1: it changes from $^{1,4}B \rightarrow [^4H_5/^4E]^{\ddagger} \rightarrow {}^4C_1 \leftrightarrow B_{3,O}$ during the reaction, suggesting a conformational pathway different from that drawn from a simple interpretation of Stoddart's pseudorotational itinerary.[21] This provides evidence of complex conformational behavior in glycoside hydrolases that utilize a substrate-assisted catalytic mechanism.

Asp142 was found to be important in stabilizing the transition state and the intermediate, by electrostatic interactions. Modeling of the D142N mutant supports the conclusion drawn from site-directed mutagenesis results that its mechanism is similar to that of the wild type. Comparison of the mutant with the wild type provides evidence of the role of Asp142 in transition state stabilization. Taken together, our findings provide insight into the reaction mechanism of the GH18 chitinases, which may further apply to other related GH enzymes utilizing the substrate-assisted mechanism.

ASSOCIATED CONTENT

Supporting Information. Analysis of root-mean-square deviation, distance, and structure during the unrestrained and restrained MD simulations for the wild type and the D142N mutant (Figures S1 and S2), PESs obtained with AM1-CHARMM22 and PM3CARB1-CHARMM22 QM/MM methods (Figure S3), including contour plots (Figure S4) of four PESs calculated at the B3LYP/6-31+G(d)//PM3CARB1-CHARMM22 level, and corresponding QM/MM energies for TS, EI1, and EI2 with respect to the energy of the reactant (Table S1), MM parameters for NAG used in the MD simulations and QM/MM calculations (Table S2), Mulliken charge analysis (Tables S3 and S4), and HOMO for the optimized TS structure (Figure S5). This material is available free of charge via the Internet at http://pubs.acs.org.

AUTHOR INFORMATION

Corresponding Author

*A.J.M.: telephone, +44 (0)117 928 9097; fax, +44 (0)117 925 1295; e-mail, adrian.mulholland@bristol.ac.uk. J.J.: telephone, +66 (0) 81 284 0207; e-mail, jitrayut.018@gmail.com.

Funding Sources

This research was supported by the Office of the Higher Education Commission, Thailand, under the program Strategic Scholarships for Frontier Research Network for the Joint Ph.D. Program (Grant CHE-PhD-SW/54/2549) Thai Doctoral degree and in part by the Center for Innovation in Chemistry (PERCH-CIC), Commission on Higher Education, Ministry of Education and Graduate School, Chiang Mai University. A.J.M. is an EPSRC Leadership Fellow and thanks EPSRC and (with H.A.R.) BBSRC for support.

■ ACKNOWLEDGMENT

We thank the reviewers for their constructive comments.

■ ABBREVIATIONS

QM/MM, quantum mechanics/molecular mechanics; GH, glycoside hydrolase; ChiB, chitinase B; ES, enzyme−substrate; TS, transition state; EI, intermediate; NAG, *N*-acetylglucosamine; PES, potential energy surface; PDB, Protein Data Bank; ABNR, Adopted Basis Newton−Raphson; MD, molecular dynamics; RC, reaction coordinate; DFT, density functional theory.

■ REFERENCES

(1) Carbohydrates and glycobiology (special issue) (2001) *Science*, Vol. 291, American Association for the Advancement of Science, Washington, DC.

(2) Cantarel, B. L., Coutinho, P. M., Rancurel, C., Bernard, T., Lombard, V., and Henrissat, B. (2009) The Carbohydrate-Active EnZymes database (CAZy): An expert resource for Glycogenomics. *Nucleic Acids Res. 37*, D233–D238.

(3) Davies, G., and Henrissat, B. (1995) Structures and mechanisms of glycosyl hydrolases. *Structure 3*, 853–859.

(4) Stick, R. V., and Williams, S. J. (2009) Enzymatic cleavage of glycosides: Mechanism, inhibition and synthetic applications. In *Carbohydrates: The essential molecules of life* (Stick, R. V., and Williams, S. J., Eds.) 2nd ed., pp 253−284, Elsevier, Oxford, U.K.

(5) Vocadlo, D. J., and Davies, G. J. (2008) Mechanistic insights into glycosidase chemistry. *Curr. Opin. Chem. Biol. 12*, 539–555.

(6) Van Aalten, D. M. F., Komander, D., Synstad, B., Gaseidnes, S., Peter, M. G., and Eijsink, V. G. H. (2001) Structural insights into the catalytic mechanism of a family 18 exo-chitinase. *Proc. Natl. Acad. Sci. U.S.A. 98*, 8979–8984.

(7) Brameld, K. A., and Goddard, W. A., III (1998) Substrate distortion to a boat conformation at subsite −1 is critical in the mechanism of family 18 chitinases. *J. Am. Chem. Soc. 120*, 3571–3580.

(8) Tews, I., Terwisscha van Scheltinga, A. C., Perrakis, A., Wilson, K. S., and Dijkstra, B. W. (1997) Substrate-assisted catalysis unifies two families of chitinolytic enzymes. *J. Am. Chem. Soc. 119*, 7954–7959.

(9) Bowman, A. L., Grant, I. M., and Mulholland, A. J. (2008) QM/MM simulations predict a covalent intermediate in the hen egg white lysozyme reaction with its natural substrate. *Chem. Commun.*, 4425–4427.

(10) Vocadlo, D. J., Mayer, C., He, S., and Withers, S. G. (2000) Mechanism of action and identification of Asp242 as the catalytic nucleophile of *Vibrio furnisii* N-acetyl-β-D-glucosaminidase using 2-acetamido-2-deoxy-5-fluoro-α-L-idopyranosyl fluoride. *Biochemistry 39*, 117–126.

(11) Vocadlo, D. J., Davies, G. J., Laine, R., and Withers, S. G. (2001) Catalysis by hen egg-white lysozyme proceeds via a covalent intermediate. *Nature 412*, 835–839.

(12) Huet, J., Rucktooa, P., Clantin, B., Azarkan, M., Looze, Y., Villeret, V., and Wintjens, R. (2008) X-ray structure of papaya chitinase reveals the substrate binding mode of glycosyl hydrolase family 19 chitinases. *Biochemistry 47*, 8283–8291.

(13) Liu, F., Iqbal, K., Grundke-Iqbal, I., Hart, G. W., and Gong, C. X. (2004) O-GlcNAcylation regulates phosphorylation of tau: A mechanism involved in Alzheimer's disease. *Proc. Natl. Acad. Sci. U.S.A. 101*, 10804–10809.

(14) Abbott, D. W., Macauley, M. S., Vocadlo, D. J., and Boraston, A. B. (2009) *Streptococcus pneumoniae* endohexosaminidase D, structural and mechanistic insight into substrate-assisted catalysis in family 85 glycoside hydrolases. *J. Biol. Chem. 284*, 11676–11689.

(15) Macauley, M. S., Whitworth, G. E., Debowski, A. W., Chin, D., and Vocadlo, D. J. (2005) O-GlcNAcase uses substrate-assisted catalysis: Kinetic analysis and development of highly selective mechanism-inspired inhibitors. *J. Biol. Chem. 280*, 25313–25322.

(16) Mark, B. L., Vocadlo, D. J., Knapp, S., Triggs-Raine, B. L., Withers, S. G., and James, M. N. (2001) Crystallographic evidence for substrate-assisted catalysis in a bacterial β-hexosaminidase. *J. Biol. Chem. 276*, 10330–10337.

(17) Cetinbas, N., Macauley, M. S., Stubbs, K. A., Drapala, R., and Vocadlo, D. J. (2006) Identification of Asp174 and Asp175 as the key catalytic residues of human O-GlcNAcase by functional analysis of site-directed mutants. *Biochemistry 45*, 3835–3844.

(18) Synstad, B., Gaseidnes, S., van Aalten, D. M. F., Vriend, G., Nielsen, J. E., and Eijsink, V. G. H. (2004) Mutational and computational analysis of the role of conserved residues in the active site of a family 18 chitinase. *Eur. J. Biochem. 271*, 253–262.

(19) Williams, S. J., Mark, B. L., Vocadlo, D. J., James, M. N. G., and Withers, S. G. (2002) Aspartate 313 in the *Streptomyces plicatus* hexosaminidase plays a critical role in substrate-assisted catalysis by orienting the 2-acetamido group and stabilizing the transition state. *J. Biol. Chem. 277*, 40055–40065.

(20) Greig, I. R., Zahariev, F., and Withers, S. G. (2008) Elucidating the nature of the *Streptomyces plicatus* β-hexosaminidase-bound intermediate using ab initio molecular dynamics simulations. *J. Am. Chem. Soc. 130*, 17620–17628.

(21) Stoddart, J. F. (1971) *Stereochemistry of carbohydrates*, Wiley-Interscience, Toronto.

(22) Lonsdale, R., Ranaghan, K. E., and Mulholland, A. J. (2010) Computational enzymology. *Chem. Commun. 46*, 2354–2372.

(23) Warshel, A., and Levitt, M. (1976) Theoretical studies of enzymic reactions: Dielectric, electrostatic and steric stabilization of the carbonium ion in the reaction of lysozyme. *J. Mol. Biol. 103*, 227–249.

(24) Ranaghan, K. E., and Mulholland, A. J. (2010) Investigations of enzyme-catalysed reactions with combined quantum mechanics/molecular mechanics (QM/MM) methods. *Int. Rev. Phys. Chem. 29*, 65–133.

(25) Petersen, L., Ardevol, A., Rovira, C., and Reilly, P. J. (2009) Mechanism of cellulose hydrolysis by inverting GH8 endoglucanases: A QM/MM metadynamics study. *J. Phys. Chem. B 113*, 7331–7339.

(26) Soliman, M. E. S., Pernia, J. J. R., Greig, I. R., and Williams, I. H. (2009)Mechanism of glycoside hydrolysis: A comparative QM/MM molecular dynamics analysis for wild type and Y69F mutant retaining xylanases. *Org. Biomol. Chem. 7*, 5236–5244.

(27) Soliman, M. E. S., Ruggiero, G. D., Pernia, J. J. R., Greig, I. R., and Williams, I. H. (2009) Computational mutagenesis reveals the role of active-site tyrosine in stabilising a boat conformation for the substrate: QM/MM molecular dynamics studies of wild-type and mutant xylanases. *Org. Biomol. Chem. 7*, 460–468.

(28) Bras, N. F., Fernandes, P. A., and Ramos, M. J. (2009) QM/MM studies on the β-galactosidase catalytic mechanism: Hydrolysis and transglycosylation reactions. *J. Chem. Theory Comput. 6*, 421–433.

(29) Liu, J., Wang, X., and Xu, D. (2010) QM/MM study on the catalytic mechanism of cellulose hydrolysis catalyzed by cellulase Cel5A from *Acidothermus cellulolyticus*. *J. Phys. Chem. B 114*, 1462–1470.

(30) Petersen, L., Ardevol, A., Rovira, C., and Reilly, P. J. (2010) Molecular mechanism of the glycosylation step catalyzed by Golgi α-mannosidase II: A QM/MM metadynamics investigation. *J. Am. Chem. Soc. 132*, 8291–8300.

(31) van der Kamp, M. W., Shaw, K. E., Woods, C. J., and Mulholland, A. J. (2008) Biomolecular simulation and modelling: Status, progress and prospects. *J. R. Soc. Interface 5*, S173–S190.

(32) Harris, W. H., and Levy, J. S. (1975) *Chitin*, Columbia University Press, New York.

(33) Houston, D. R., Shiomi, K., Arai, N., Omura, S., Peter, M. G., Turberg, A., Synstad, B., Eijsink, V. G., and van Aalten, D. M. (2002) High-resolution structures of a chitinase complexed with natural product cyclopentapeptide inhibitors: Mimicry of carbohydrate substrate. *Proc. Natl. Acad. Sci. U.S.A. 99*, 9127–9132.

(34) Horn, S. J., Sikorski, P., Cederkvist, J. B., Vaaje-Kolstad, G., Soerlie, M., Synstad, B., Vriend, G., Vaerum, K. M., and Eijsink, V. G. H. (2006) Costs and benefits of processivity in enzymatic degradation of recalcitrant polysaccharides. *Proc. Natl. Acad. Sci. U.S. A. 103*, 18089–18094.

(35) Vaaje-Kolstad, G., Houston, D. R., Rao, F. V., Peter, M. G., Synstad, B., van Aalten, D. M., and Eijsink, V. G. (2004) Structure of the D142N mutant of the family 18 chitinase ChiB from *Serratia marcescens* and its complex with allosamidin. *Biochim. Biophys. Acta 1696*, 103–111.

(36) Hermann, J. C., Hensen, C., Ridder, L., Mulholland, A. J., and Höltje, H. D. (2005) Mechanisms of antibiotic resistance: QM/MM modeling of the acylation reaction of a class A β-lactamase with benzylpenicillin. *J. Am. Chem. Soc. 127*, 4454–4465.

(37) Lodola, A., Mor, M., Hermann, J. C., Tarzia, G., Piomelli, D., and Mulholland, A. J. (2005) QM/MM modelling of oleamide hydrolysis in fatty acid amide hydrolase (FAAH) reveals a new mechanism of nucleophile activation. *Chem. Commun.,* 4399–4401.

(38) Ranaghan, K. E., Ridder, L., Szefczyk, B., Sokalski, W. A., Hermann, J. C., and Mulholland, A. J. (2003) Insights into enzyme catalysis from QM/MM modelling: Transition state stabilization in chorismate mutase. *Mol. Phys. 101*, 2695–2714.

(39) Krokeide, I.-M., Synstad, B., Gaseidnes, S., Horn, S. J., Eijsink, V. G. H., and Sorlie, M. (2007) Natural substrate assay for chitinases using high-performance liquid chromatography: A comparison with existing assays. *Anal. Biochem. 363*, 128–134.

(40) Vasella, A., Davies Gideon, J., and Bohm, M. (2002) Glycosidase mechanisms. *Curr. Opin. Chem. Biol. 6*, 619–629.

(41) Henrissat, B., Sulzenbacher, G., and Bourne, Y. (2008) Glycosyltransferases, glycoside hydrolases: Surprise, surprise. *Curr. Opin. Struct. Biol. 18*, 527–533.

(42) Berman, H. M., Westbrook, J., Feng, Z., Gilliland, G., Bhat, T. N., Weissig, H., Shindyalov, I. N., and Bourne, P. E. (2000) The Protein Data Bank. *Nucleic Acids Res. 28*, 235–242.

(43) Brunger, A. T., and Karplus, M. (1988)Polar hydrogen positions in proteins: Empirical energy placement and neutron diffraction comparison. *Proteins: Struct., Funct., Genet. 4*, 148–156.

(44) Bas, D. C., Roger, D. M., and Jensen, J. H. (2008) Very fast prediction and rationalization of pKa values for protein-ligand complexes. *Proteins: Struct., Funct., Bioinf. 73*, 765–783.

(45) Vriend, G. (1990) WHAT IF: A molecular modeling and drug design program. *J. Mol. Graphics 8*, 29, 52−56.

(46) MacKerell, A. D., Jr., Bashford, D., Bellott, M., Dunbrack, R. L., Evanseck, J. D., Field, M. J., Fischer, S., Gao, J., Guo, H., Ha, S., Joseph-McCarthy, D., Kuchnir, L., Kuczera, K., Lau, F. T. K., Mattos, C., Michnick, S., Ngo, T., Nguyen, D. T., Prodhom, B., Reiher, W. E., III, Roux, B., Schlenkrich, M., Smith, J. C., Stote, R., Straub, J., Watanabe, M., Wiorkiewicz-Kuczera, J., Yin, D., and Karplus, M. (1998) All-atom empirical potential for molecular modeling and dynamics studies of proteins. *J. Phys. Chem. B 102*, 3586–3616.

(47) Foloppe, N., and MacKerell, J. A. D. (2000) All-atom empirical force field for nucleic acids: I. Parameter optimization based on small molecule and condensed phase macromolecular target data. *J. Comput. Chem. 21*, 86–104.

(48) MacKerell, A. D., Wiorkiewicz-Kuczera, J., and Karplus, M. (2002) An all-atom empirical energy function for the simulation of nucleic acids. *J. Am. Chem. Soc. 117*, 11946–11975.

(49) Woods, R. J., Dwek, R. A., Edge, C. J., and Fraser-Reid, B. (1995) Molecular mechanical and molecular dynamical simulations of glycoproteins and oligosaccharides. 1. GLYCAM_93 parameter development. *J. Phys. Chem. 99*, 3832–3846.

(50) Brooks, B. R., Bruccoleri, R. E., Olafson, B. D., States, D. J., Swaminathan, S., and Karplus, M. (1983) CHARMM: A program for macromolecular energy, minimization, and dynamics calculations. *J. Comput. Chem. 4*, 187–217.

(51) Bowman, A. L., Ridder, L., Rietjens, I. M., Vervoort, J., and Mulholland, A. J. (2007) Molecular determinants of xenobiotic metabolism: QM/MM simulation of the conversion of 1-chloro-2,4-dinitrobenzene catalyzed by M1-1 glutathione S-transferase. *Biochemistry 46*, 6353–6363.

(52) Ranaghan, K. E., Ridder, L., Szefczyk, B., Sokalski, W. A., Hermann, J. C., and Mulholland, A. J. (2004) Transition state stabilization and substrate strain in enzyme catalysis: Ab initio QM/MM modelling of the chorismate mutase reaction. *Org. Biomol. Chem. 2*, 968–980.

(53) Shaw, K. E., Woods, C. J., and Mulholland, A. J. (2010) Compatibility of quantum chemical methods and empirical (MM) water models in quantum mechanics/molecular mechanics liquid water simulations. *J. Phys. Chem. Lett. 1*, 219–223.

(54) Brooks, C. L., III, and Karplus, M. (1983) Deformable stochastic boundaries in molecular dynamics. *J. Chem. Phys. 79*, 6312–6325.

(55) Ryckaert, J.-P., Ciccotti, G., and Berendsen, H. J. C. (1977) Numerical integration of the cartesian equations of motion of a system with constraints: Molecular dynamics of n-alkanes. *J. Comput. Phys. 23*, 327–341.

(56) Lodola, A., Sirirak, J., Fey, N., Rivara, S., Mor, M., and Mulholland, A. J. (2010) Structural fluctuations in enzyme-catalyzed reactions: Determinants of reactivity in fatty acid amide hydrolase from multivariate statistical analysis of quantum mechanics/molecular mechanics paths. *J. Chem. Theory Comput. 6*, 2948–2960.

(57) Lodola, A., Mor, M., Zurek, J., Tarzia, G., Piomelli, D., Harvey, J. N., and Mulholland, A. J. (2007) Conformational effects in enzyme catalysis: Reaction via a high energy conformation in fatty acid amide hydrolase. *Biophys. J. 92*, L20–L22.

(58) Dewar, M. J. S., Zoebisch, E. G., Healy, E. F., and Stewart, J. J. P. (1985) Development and use of quantum mechanical molecular models. 76. AM1: A new general purpose quantum mechanical molecular model. *J. Am. Chem. Soc. 107*, 3902–3909.

(59) McNamara, J. P., Muslim, A.-M., Abdel-Aal, H., Wang, H., Mohr, M., Hillier, I. H., and Bryce, R. A. (2004) Towards a quantum mechanical force field for carbohydrates: A reparametrized semi-empirical MO approach. *Chem. Phys. Lett. 394*, 429–436.

(60) McNamara, J. P., and Hillier, I. H. (2009) Towards an accurate semi-empirical molecular orbital treatment of covalent and non-covalent biological interactions. In *Multi-scale quantum models for biocatalysis: Modern techniques and applications* (York, D. M., and Lee, T. S., Eds.) pp 105−136, Springer, London.

(61) Reuter, N., Dejaegere, A., Maigret, B., and Karplus, M. (2000) Frontier bonds in QM/MM methods: A comparison of different approaches. *J. Phys. Chem. A 104*, 1720–1735.

(62) Rodriguez, A., Oliva, C., Gonzalez, M., van der Kamp, M., and Mulholland, A. J. (2007) Comparison of different quantum mechanical/molecular mechanics boundary treatments in the reaction of the hepatitis C virus NS3 protease with the NS5A/5B substrate. *J. Phys. Chem. B 111*, 12909–12915.

(63) van der Kamp, M. W., Zurek, J., Manby, F. R., Harvey, J. N., and Mulholland, A. J. (2010) Testing high-level QM/MM methods for modeling enzyme reactions: Acetyl-CoA deprotonation in citrate synthase. *J. Phys. Chem. B 114*, 11303–11314.

(64) Ridder, L., Mulholland, A. J., Rietjens, I. M. C. M., and Vervoort, J. (2000) A quantum mechanical/molecular mechanical study of the hydroxylation of phenol and halogenated derivatives by phenol hydroxylase. *J. Am. Chem. Soc. 122*, 8728–8738.

(65) McCammon, J. A., and Harvey, S. C. (1987) *Dynamics of proteins and nucleic acids*, Cambridge University Press, Cambridge, U.K.

(66) Lodola, A., Mor, M., Sirirak, J., and Mulholland, A. J. (2009) Insights into the mechanism and inhibition of fatty acid amide hydrolase from quantum mechanics/molecular mechanics (QM/MM) modelling. *Biochem. Soc. Trans. 37*, 363–367.

(67) Rungrotmongkol, T., Decha, P., Sompornpisut, P., Malaisree, M., Intharathep, P., Nunthaboot, N., Udommaneethanakit, T., Aruksakunwong, O., and Hannongbua, S. (2009) Combined QM/MM mechanistic study of

the acylation process in furin complexed with the H5N1 avian influenza virus hemagglutinin's cleavage site. *Proteins: Struct., Funct., Bioinf. 76*, 62–71.

(68) Garcia-Viloca, M., Gao, J., Karplus, M., and Truhlar, D. G. (2004) How enzymes work: Analysis by modern rate theory and computer simulations. *Science 303*, 186–195.

(69) Claeyssens, F., Harvey, J. N., Manby, F. R., Mata, R. A., Mulholland, A. J., Ranaghan, K. E., Schütz, M., Thiel, S., Thiel, W., and Werner, H. J. (2006) High-accuracy computation of reaction barriers in enzymes. *Angew. Chem., Int. Ed. 45*, 6856–6859.

(70) Sinnott, M. L. (1984) On the antiperiplanar lone pair hypothesis and its application to catalysis by glycosidases. *Biochem. J. 224*, 817–821.

(71) Deslongchamps, P. (1993) Intramolecular strategies and stereoelectronic effects. Glycosides hydrolysis revisited. *Pure Appl. Chem. 65*, 1161–1178.

(72) Hermann, J. C., Pradon, J., Harvey, J. N., and Mulholland, A. J. (2009)High level QM/MM modeling of the formation of the tetrahedral intermediate in the acylation of wild type and K73A mutant TEM-1 class A β-lactamase. *J. Phys. Chem. A 113*, 11984–11994.

(73) Claeyssens, F., Ranaghan, K. E., Manby, F. R., Harvey, J. N., and Mulholland, A. J. (2005) Multiple high-level QM/MM reaction paths demonstrate transition-state stabilization in chorismate mutase: Correlation of barrier height with transition-state stabilization. *Chem. Commun.,* 5068–5070.

(74) Hermann, J. C., Ridder, L., Höltje, H. D., and Mulholland, A. J. (2006) Molecular mechanisms of antibiotic resistance: QM/MM modelling of deacylation in a class A β-lactamase. *Org. Biomol. Chem. 4*, 206–210.

(75) Ridder, L., Rietjens, I. M., Vervoort, J., and Mulholland, A. J. (2002) Quantum mechanical/molecular mechanical free energy simulations of the glutathione S-transferase (M1-1) reaction with phenanthrene 9,10-oxide. *J. Am. Chem. Soc. 124*, 9926–9936.

(76) Garcia-Viloca, M., Truhlar, D. G., and Gao, J. (2003) Importance of substrate and cofactor polarization in the active site of dihydrofolate reductase. *J. Mol. Biol. 327*, 549–560.